Spin-Orbit Torque Switching of Compensated Ferrimagnetic Cobalt-Terbium Alloys

by

Joseph T. Finley

B.S. Engineering Physics
B.S. Electrical Engineering and Computer Science
University of California Berkeley 2014

Submitted to the Department of Electrical Engineering and Computer Science in partial fulfillment of the requirements for the degree of

Master of Science in Electrical Engineering and Computer Science

at the

MASSACHUSETTS INSTITUTE OF TECHNOLOGY

June 2017

Signature of Author: Signature redacted
Department of Electrical Engineering and Computer Science
May 19, 2017

Certified by: Signature redacted
Marc A. Baldo
Professor of Electrical Engineering and Computer Science / Director of RLE
Thesis Supervisor

Accepted by: Signature redacted
Leslie A. Kolodziejski
Professor of Electrical Engineering and Computer Science
Chair, Department Committee on Graduate Students

Spin-Orbit Torque Switching of Compensated Ferrimagnetic Cobalt-Terbium Alloys

by

Joseph T. Finley

B.S. Engineering Physics
B.S. Electrical Engineering and Computer Science
University of California Berkeley 2014

Submitted to the Department of Electrical Engineering and Computer Science on May 19, 2017,
in partial fulfillment of the requirements for the degree of
Master of Science in Electrical Engineering and Computer Science.

ABSTRACT

Spintronic devices promise to be an energy efficient alternative to complementary metal oxide semiconductor devices for logic and memory. However, in order to be more competitive, further reductions in switching energy and switching speed are needed. Recently, there has been interest in using antiferromagnetically coupled materials instead of ferromagnetic materials to store information. Compared with ferromagnetic materials, antiferromagnetically coupled systems exhibit faster dynamics and are more stable against external magnetic field perturbations, which could potentially enable spintronic devices with higher speed and density. Despite the potential advantages of information storage in antiferromagnetically coupled materials, it remains uncertain whether one can efficiently control the magnetic state because of the cancelled net magnetic moment.

This thesis reports spin-orbit torque induced magnetization switching of ferrimagnetic $Co_{1-x}Tb_x$ thin films with perpendicular magnetic anisotropy. By varying the relative concentrations of the two atomic species, one can reach compensation points where the net magnetic moment or angular momentum goes to zero. We demonstrate current induced switching in all of the studied film compositions, including those near the magnetization compensation point. We then quantify the spin-orbit torque induced effective field, where we find that close to the compensation point, there is a divergent behavior that scales with the inverse of the magnetization, consistent with angular momentum conservation. The large effective spin-orbit torque, previously demonstrated fast dynamics, and small net magnetization in these ferrimagnetic systems promise spintronic devices that are faster and more scalable than traditional ferromagnetic systems.

Thesis Supervisor: Marc A. Baldo
Title: Professor of Electrical Engineering and Computer Science

Acknowledgements

I would like to thank my advisors Marc Baldo and Luqiao Liu, and my labmates, friends, family, and wife.

Contents

List of Figures

List of Tables

Chapter 1

Introduction

The future of Moore's Law is uncertain, and one of the fundamental weaknesses of traditional complementary metal oxide semiconductor (CMOS) devices is the power dissipation. For this reason, researchers are searching for beyond CMOS energy efficient devices. The field of spintronics aims to use electron spin, instead of charge, to store, control, and read information. So far, spintronics devices have been shown to have low power dissipation relative to other emerging logic [1] and memory devices [2]. These devices are based upon magnetic tunnel junctions (MTJ) which consists of two magnetic layers separated by a thin insulating layer. When the two magnetic layers have magnetic moments in the same direction, the tunneling resistance through the junction is low (On-state) and when the two layers have magnetic moments in the opposite direction, the resistance is high (Off-state). Due to the hysteretic nature of magnetic materials, many of the potential spintronics devices are non-volatile, meaning they retain their state when powered off, which is ideal for memory devices. In addition to the classic Von Neumann computing architecture, emerging architectures based upon neuromorphic computing can greatly benefit from spintronics-based devices. Nonvolatile MTJ devices can be employed in neuromorphic systems that aim to conserve energy and increase throughput by putting memory directly in logic [3] or as nonlinear, nonvolatile function devices for convolution networks [4].

Whether considering MTJ-based devices for Von Neumann or neuromorphic architectures, one weakness is the delay, or switching speed, when compared with CMOS devices. In order to overcome this weakness, new magnetic materials that possess faster dynamics need to be studied.

1.1 Spin Torque

In 1996 Slonczewski and Berger independently predicted that when a spin current impinges on a magnetic material, the angular momentum of the spin current can be transferred to the magnetic material, exciting magnetic oscillations [5,6]. This prediction of spin-transfer torque (STT) was later experimentally verified [7,8] in spin-valve structures consisting to magnetic layers separated by a nonmagnetic metal layer with small spin scattering (Fig. 1.1). It was shown that if the spin-current density was large enough to overcome damping, then full magnetic switching was possible. Qualitatively, the induced magnetic dynamics and switching occurs in a spin-valve structure through the following process. First, electrons enter the "pinned" magnetic layer due to the presence of an electronic current. These conduction electrons experience angular momentum transfer, causing the electrons to have their spin aligned in the same direction as the pinned layer moment, which results in a spin-polarized current. The spin-polarized current enters the non-magnetic layer and then impinges on "free" layer. Assuming the free layer has its magnetic orientation opposite to the pinned layer direction, the spin-polarized current transfers its angular momentum (and the free layer transfers its angular momentum to

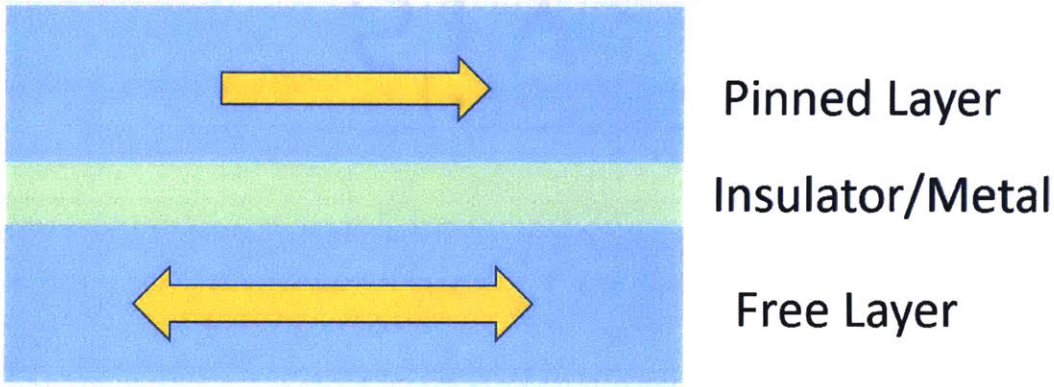

Figure 1.1: Basic structure of spin valve (non-magnetic metal spacer) and magnetic tunnel junction (insulating barrier).

the conduction electrons), which excites dynamics and potentially causes the free layer to reverse its moment direction. If a current is applied in the opposite direction, then the free layer generates a spin-polarized current that impinges on the pinned layer. Due to the different scattering rates of electrons of opposite spin directions, the amount of electrons that are transmitted through the pinned layer depends on moment direction of the free layer. If the free layer and the pinned layer are aligned in the same direction, then electrons polarized antiparallel to the free layer are more likely to be reflected. Through diffusion, these electrons impinge on the free layer and exert a torque that prefers antiparallel alignment of the free and pinned layers. To summarize, currents of opposite sign will generate parallel and anti-parallel alignment. Several years later, spin-transfer torque switching of MTJs was demonstrated [9]. The switching mechanism in an MTJ is analogous to the case in spin-valves, however instead of relying upon drift and diffusion, tunneling current generates the angular momentum transfer. Furthermore,

STT has been shown to influence domain wall dynamics in magnetic wires, including domain wall motion above a critical current [10].

Magnetization dynamics can be described using the Landau–Lifshitz–Gilbert (LLG) equation:

$$\frac{d\hat{\boldsymbol{m}}}{dt} = -\gamma\left(\hat{\boldsymbol{m}} \times \boldsymbol{H}_{eff}\right) + \alpha\left(\hat{\boldsymbol{m}} \times \frac{d\hat{\boldsymbol{m}}}{dt}\right). \tag{1.1}$$

Here $\hat{\boldsymbol{m}}$ is a unit vector in the direction of the magnetic moment, γ is the gyromagnetic ratio, $\hat{\boldsymbol{H}}_{eff}$ is the effective magnetic field, which includes the anisotropy field, the demagnetization field, and any applied external fields, and α is the Gilbert damping parameter. When considering spin-transfer torque in spin-valves and MTJ structures, the LLG equation becomes [5,11]:

$$\frac{d\hat{\boldsymbol{m}}}{dt} = -\gamma\left(\hat{\boldsymbol{m}} \times \boldsymbol{H}_{eff}\right) + \alpha\left(\hat{\boldsymbol{m}} \times \frac{d\hat{\boldsymbol{m}}}{dt}\right) - \gamma\eta\frac{\hbar J_e}{2e\mu_0 M_S t}\left(\hat{\boldsymbol{m}} \times \hat{\boldsymbol{m}}_{\boldsymbol{pinned}} \times \hat{\boldsymbol{m}}\right). \tag{1.2}$$

In the additional term, $\hbar$ is Planck's constant, J_e is the applied current density, t is the thickness of the free layer magnet, μ_0 is the permeability of free space, M_S is the saturation magnetization of the free layer, e is the charge of an electron, $\hat{\boldsymbol{m}}_{\boldsymbol{pinned}}$ is the magnetic moment direction of the pinned layer, and η is the effective spin polarization, which can depend on the angle between the free and pinned layer magnetic moments. As seen in Fig. 1.2a, STT acts either in the same direction or the opposite direction as the torque induced by damping. For this reason this torque is referred to as the anti-damping torque or the Slonczewski torque. Fig. 1.2b demonstrates the processional path the free layer moment takes when switching when acted upon by an anti-damping torque.

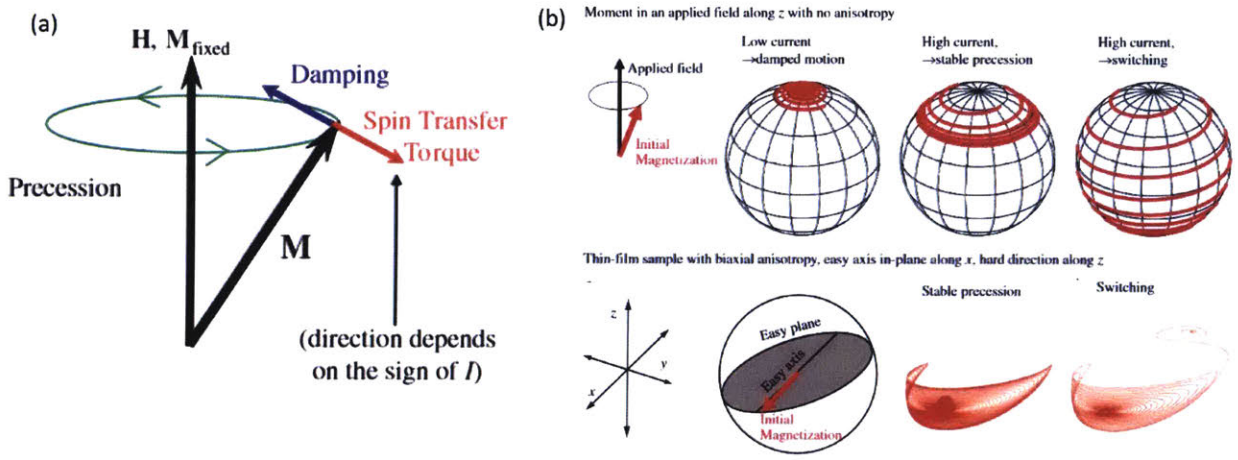

Figure 1.2 Spin Transfer Torque Dynamics: (a) STT acts perpendicularly to the precession, either opposing or adding with the damping depending in the current direction. (b) Top demonstrates the case where damping is larger than the STT, damping and STT are matched and precession occurs, and the case where STT is large enough to induce switching. Bottom shows the case of a thin-film with biaxial anisotropy, which has to overcome the easy plane and hard axis anisotropy for switching to occur. Figure is reproduced from [11].

The analytical expression for the critical current for STT anti-damping switching of an in-plane spin-valve or MTJ is [12]:

$$I_c = \frac{2e\mu_0 M_S V}{\hbar\eta}\left(\widehat{\boldsymbol{H}}_c + \widehat{\boldsymbol{H}}_d\right). \tag{1.3}$$

Here V is the volume of the free layer (note that the critical current density only depends on the thickness of the free layer), $\widehat{\boldsymbol{H}}_c$ is the in-plane coercive field which can depend on shape and magneto-crystalline anisotropy, and $\widehat{\boldsymbol{H}}_d$ is the effective out of plane anisotropy field due to the demagnetization field. Because the critical current density is directly proportional to the free layer thickness, free layers are designed to only be on the order of several nanometers thick. Ultrathin magnetic films possess large demagnetization fields that can be 2 to 3 orders of

magnitude larger than the coercive field. As seen in Fig. 1.2b, antidumping switching causes the free layer moment to process out of plane and must overcome the demagnetization field. Furthermore, only the coercive field plays a role in the thermal stability of the free layer, which is typically chosen so that room temperature thermal switching time is on the order of 10 years. In the case of STT switching of magnetic films with perpendicular magnetic anisotropy (PMA), the critical current only depends on the coercive field, which also determines the thermal stability. Therefore using free layers with is preferred for reducing the switching energy.

In order to increase the switching time in STT devices, one approach is to apply larger spin currents. In the short pulse length regime (less than several nanoseconds), the switching time decreases with increasing electrical current density that is larger than the critical current [12]. However, the inverse is also true: at shorter current pulse lengths, the critical current increases. The decrease in switching time requires larger power and energy dissipation. Another method to decrease the switching time in STT devices is to reduce what is referred to as the incubation time [12–14]. By examining the LLG equation including STT, one can notice that if the free layer and fixed layer and perfectly anti-parallel, there is no angular momentum transfer. In order for momentum transfer to occur, a thermally-induced random perturbation is required to induce an orthogonal component between the free and pinned layers. Due to the randomness of this thermal perturbation, the switching probably for short pulses can be less than 1. To overcome this effect, a magnetic layer with PMA can be inserted next to free layer to act as an out of plane polarizer causing the free layer to tilt. Purposefully tilting the free layer eliminates the stochasticity of switching by eliminating the random incubation time. Furthermore the starting position of the free layer relative to the pinned layer determines the number of processions the

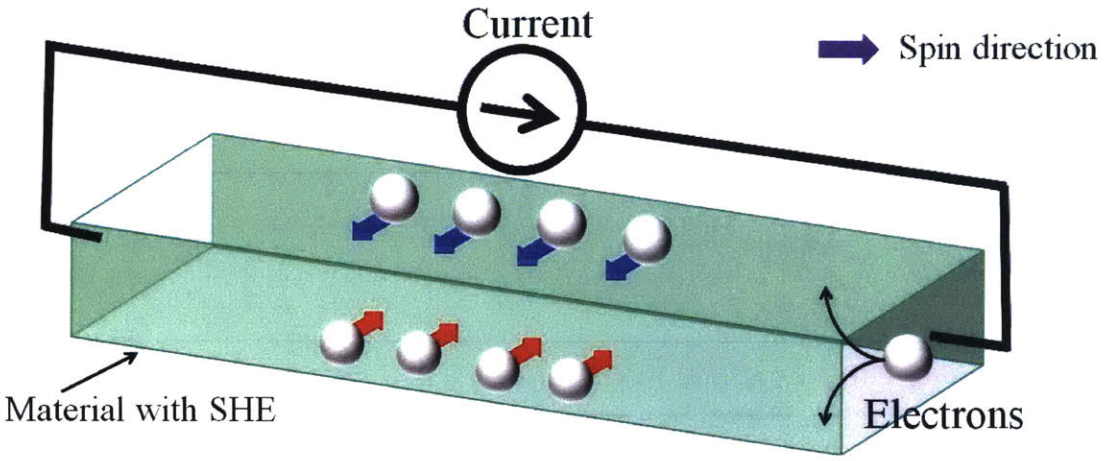

Figure 1.3: Spin Hall effect. By flowing an electrical current, due to extrinsic or intrinsic mechanisms, a spin current is generated and spin accumulation occurs at the surface. The spin direction is perpendicular to the applied current direction and parallel to the surface.

free layer undergoes before switching. To further reduce switching times, one must find a way to increases the processional frequency of the free layer. The processional frequency and corresponding switching time is proportional to the ferromagnetic resonance (FMR) [12], which depends on the gyromagnetic ratio and anisotropy field. Exploring materials with large FMR values could be beneficial for increasing the switching time in magnetic devices.

Flowing electrons through magnetic materials is not the only way to generate spin currents electronically. Over the past several years, researchers have been exploring spin-currents generating through spin-orbit interactions in non-magnetic materials, such as the spin Hall effect (SHE) [15,16] and the Rashba-Edelstein effect [17,18]. Fig. 1.3 demonstrates how a spin current is generated from the SHE. When an electrical current flows in a material with large spin-orbit coupling, such as heavy metals or semiconductors, electrons with spin orthogonal to the current direction and parallel to the surface obtain a transverse velocity, which generates a

spin-current and spin accumulation at the surface or interface of the material. The SHE shares much of the same physics as the anomalous Hall effect (AHE) and can be a result of extrinsic mechanisms such as skew and side-jump scattering or through intrinsic mechanisms due to band structure and Berry phase [19]. The strength of the SHE is described with by the spin Hall angle θ_{SH}, which the ratio of spin current density generated to electric current density applied. The Rashba-Edelstein effect (Fig. 1.4) is a relativistic effect that is a result of broken inversion symmetry. In the reference frame of a conduction electron, an electric field resulting from a lattice potential appears as a magnetic field. This magnetic field lifts the spin degeneracy of the conduction electrons by causing a spin-dependent shift of the band structure in k-space (Fig. 1.4), resulting in a spin-accumulation when an electric current is applied. The Rashba Hamiltonian is typically written, $\widehat{\boldsymbol{H}} = \frac{\alpha_R}{\hbar}(\hat{\boldsymbol{z}} \times \hat{\boldsymbol{p}}) \cdot \hat{\boldsymbol{\sigma}}$, where α_R is the Rashba parameter, $\hat{\boldsymbol{z}}$ is the direction of the symmetry braking electric field, $\hat{\boldsymbol{p}}$ is the electron momentum, and $\hat{\boldsymbol{\sigma}}$ is the Pauli spin matrix [17].

In order to excite magnetization dynamics using the SHE or Rashba-Edelstein effect, a magnetic layer is typically placed adjacent to the spin-orbit material. The spin current and spin accumulation can lead to two different magnetic interactions. The LLG equation with these two interactions is written:

$$\frac{d\hat{\boldsymbol{m}}}{dt} = -\gamma\left(\hat{\boldsymbol{m}} \times \boldsymbol{H}_{eff}\right) + \alpha\left(\hat{\boldsymbol{m}} \times \frac{d\hat{\boldsymbol{m}}}{dt}\right) - \gamma \frac{\hbar J_s}{2e\mu_0 M_S t}(\hat{\boldsymbol{m}} \times \boldsymbol{\sigma} \times \hat{\boldsymbol{m}}) - \gamma\left(\hat{\boldsymbol{m}} \times \hat{\boldsymbol{H}}_R\right). \quad (1.4)$$

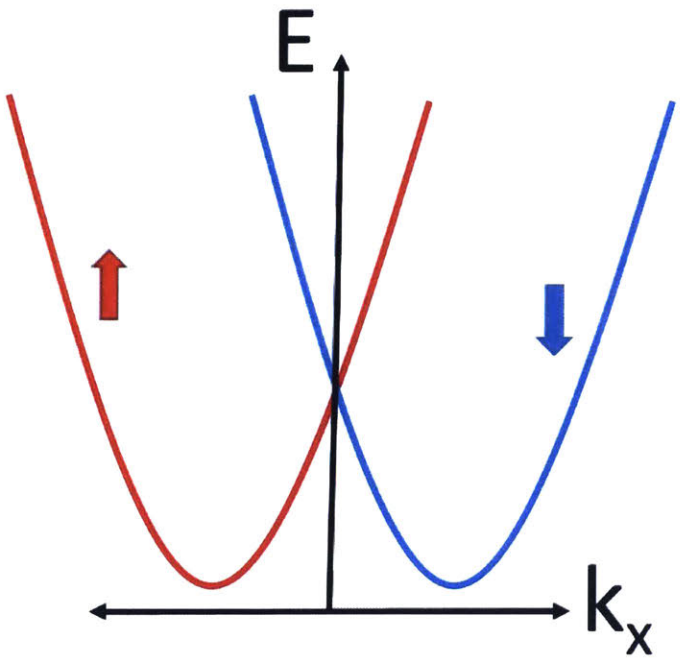

Figure 1.4: Rashba effect. Due to broke inversion symmetry, the Rashba Hamiltonian split the spin-up (red) and spin-down (blue) bands in k-space. Applying a current and shifting the fermi surface results in spin accumulation.

Here, J_S is the spin current density and is part of the Slonczewski torque term. The spin current can be due to both the SHE and Rashba effect. $\widehat{\boldsymbol{H}}_R$ is the Rashba field and is part of the term referred to as the field-like torque. The Slonczewski torque is relevant in the long spin carrier lifetime regime, while the field-like torque occurs in the short spin lifetime and is due to exchange coupling with the magnetic material and the accumulated spin at the interface.

Over the past few years a great deal of work has been done studying materials and physics of spin generation through spin-orbit interactions. The SHE has been shown to generate a large enough spin current in heavy metals such as Pt, Ta, W, etc. to switch the magnetic orientation in an adjacent in-plane ferromagnet [20,21]. The physics of this type of switching is analogous to

STT switching, however current is now applied only in the heavy metal. This can be used to create a three terminal device with an MTJ on top of a heavy metal. This device has benefit of reducing the switching energy and allows for a reduction of the current going through the MTJ, potentially increasing the endurance. The reduction in energy can be understood with the following analysis. Similar to the case of STT switching the critical current density can be written:

$$J_c = \frac{2e\mu_0 M_S t}{\hbar\theta_{SH}}\left(\widehat{\boldsymbol{H}}_c + \widehat{\boldsymbol{H}}_d\right). \tag{1.5}$$

Compared with the critical current for STT switching the only difference is the substitution of the spin Hall angle with the spin polarization. Typically θ_{SH} ~ 0.1 the heavy metals Pt and Ta, while spin polarization values can be at most 1, but typically less. Comparing the total current between the two, the area of the MTJ can be an order of magnitude larger than the area in the heavy metal wire because the wire thickness is only several nanometers. Furthermore, the resistance in the wire can also be less than the resistance through the MTJ, ultimately resulting in a reduction in the total power.

Not only has spin current generated through spin-orbit interactions been used to switching in-plane magnetic materials, but it has also been used to switch perpendicular magnetic films [22,23], as well as drive domain walls [24,25]. By symmetry, it is not possible to switch the magnetic state of a perpendicular material with a spin current that has spin orientation in-plane. Instead, a field is required to break this symmetry. To understand this, I will examine a macrospin mono-domain model and a multi-domain model. In the macrospin case (Fig. 1.5), in the absence of an external fields, the magnetic moment can lie in the $+\hat{\boldsymbol{z}}$ or $-\hat{\boldsymbol{z}}$ direction. If a spin current is injection with spin orientation in the $+\hat{\boldsymbol{x}}$ ($-\hat{\boldsymbol{x}}$) direction, then the magnetic

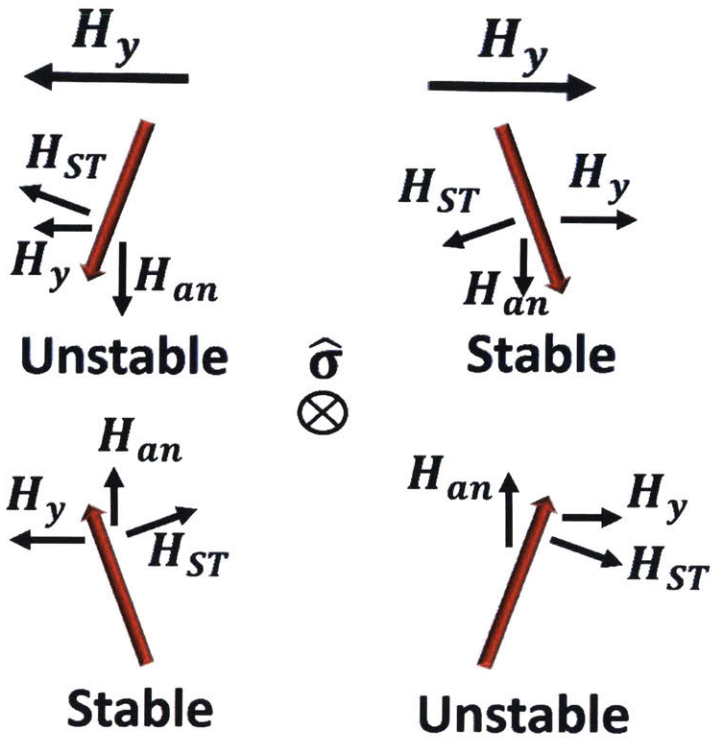

Figure 1.5: Switching phase diagram for SOT-induced switching of PMA films. For a given applied current direction and therefore injected spin direction, reversing the in-plane field reverses the equilibrium position.

moment can gain momentum in the $+\hat{x}$ ($-\hat{x}$) direction through momentum transfer. Applying a larger spin current will only generate more momentum transfer in the $\hat{x}$ direction, but does not prefer $+\hat{z}$ or $-\hat{z}$ direction. If an external field is applied, the symmetry is broken. Defining the effective field generated by the spin-torque as $H_{ST} \propto \hat{\sigma} \times \hat{m}$, then the equilibrium position can be found by balancing the anisotropy field H_{an}, the in-plane applied field H_y, and H_{ST}. Reversing the applied current direction, therefore applying a spin-torque of opposite magnitude changes the equilibrium position from down to up or up to down. Similarly, applying H_y in the opposite

direction also causes the magnetic state to switch, resulting in the switching phase diagram seen in Fig. 1.5

The spin-orbit induced spin-torque switching of PMA materials occurs at critical currents that are much smaller than those predicted assuming switching occurs at fields larger than the anisotropy field [26]. Instead it is much more likely switching occurs through domain-wall nucleation and propagation. In order for SOT driven domain wall (DW) motion to occur, the DW must be a Néel domain wall instead of a Bloch DW by symmetry [27]. Fig. 1.6 shows the case of a spin-orbit torque (SOT) acting upon a Néel DW. Here, H_{ST} acts in the perpendicular direction facilitating DW motion that prefers a magnetic orientation in the $+\hat{z}$ or $-\hat{z}$ direction depending on the chirality of the DW and the injected spin direction. In a thin magnetic layer with PMA, Bloch DWs possess lower energy than Néel DWs. However, due to the Dzyaloshinskii-Moriya interaction and spin-orbit coupling [28], stable Néel DWs are formed in heavy-metal ferromagnet bilayers with spontaneous chiralities. Therefore, in the DW regime, the application of an in-plane field can be viewed as breaking the spontaneous chiralities, and defining a set chirality and a preferred switching direction (Fig. 1.6).

The application of a static in-plane magnetic field is not ideal for practical electronic devices. However, there have been efforts to design switchable systems without an external field. First, if a Néel DW is already nucleated, then the DW can be moved using SOT without an external field. Other solutions have been used to break the symmetry of the system, such as having a gradient oxide deposited on top of the ferromagnetic material to realize field free switching [29]. More recently, researchers have been able to demonstrate field-free switching using the

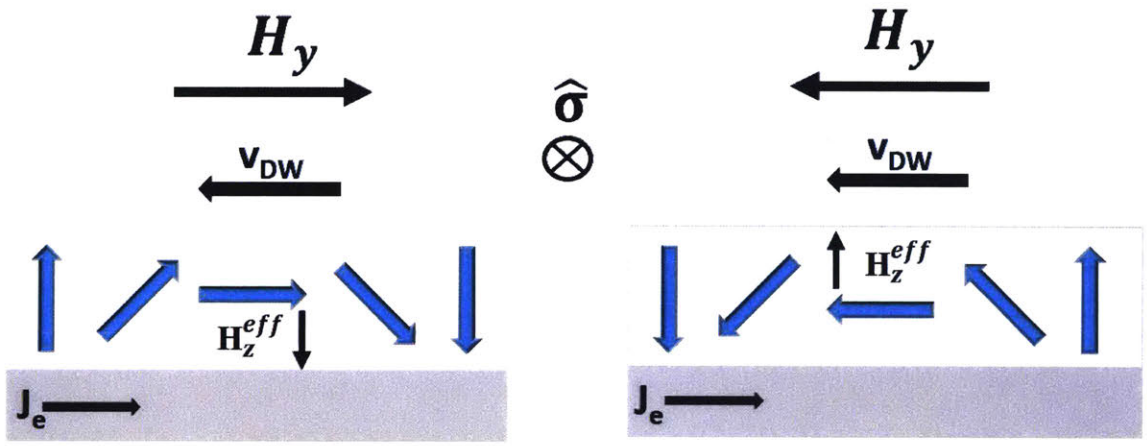

Figure 1.6: SOT-induced domain wall motion. Néel DWs of opposite chirality defined by an external field. Effective spin torque field is in opposite direction for opposite chiralities. DW velocity depends on whether DW Up-to-Down or Down-to-Up.

exchange bias of an adjacent antiferromagnetic material (which also was shown to have a large enough spin Hall angle for switching) [30,31].

In addition to realizing field-free switching, researchers are also finding new materials that can generate spin currents with increased efficiency, such as topological insulators [32–34]. Topological insulators have topologically protected spin-momentum locking, causing large effective spin Hall angles that can reduce the power consumption in spintronic devices, making them more practical overall. While the energy efficiency of generating spin currents continues to decrease and SOT switching of PMA materials has been demonstrated on the order of several hundred picoseconds [35], researchers need to continue to do more work to obtain faster switching spintronic devices to be competitive as devices in Von Neumann or neuromorphic computing architectures.

1.2 Antiferromagnetically-Coupled Materials

Up until recently, most of the work done of spin-torque induced magnetization dynamics has focused on ferromagnetic materials, with some exceptions [36,37]. However, the relevant frequencies in antiferromagnetically-coupled materials (antiferromagnetic and ferrimagnetic materials) are typically in the 10 GHz to THz regimes, much higher than ferromagnetic materials [38–41]. Although the higher frequencies promise faster switching devices, challenges remain in using spin-torque to efficiently switch the magnetic state, in addition to being able to efficiently detect the magnetic state.

Two magnetic sublattices' dynamics can be represented with the macrospin LLG equation [42]:

$$\frac{d\boldsymbol{M}_1}{dt} = -\gamma_1\left(\boldsymbol{M}_1 \times \boldsymbol{H}_{eff}\right) + \frac{\alpha_1}{M_1}\left(\boldsymbol{M}_1 \times \frac{d\boldsymbol{M}_1}{dt}\right), \tag{1.6}$$

$$\frac{d\boldsymbol{M}_2}{dt} = -\gamma_2\left(\boldsymbol{M}_2 \times \boldsymbol{H}_{eff}\right) + \frac{\alpha_2}{M_2}\left(\boldsymbol{M}_2 \times \frac{d\boldsymbol{M}_2}{dt}\right). \tag{1.7}$$

The two sublattice magnetic moments per unit volume $\boldsymbol{M}_1$ and $\boldsymbol{M}_2$have different damping coefficients and gyromagnetic ratios due to the different Lande g-factors associated with each sublattice. $\boldsymbol{H}_{eff}$ includes external fields, anisotropy fields, the demagnetization field, and couples the two sublattices through an exchange field. Assuming perfect antiferromagnetic exchange (anti-parallel sublattices) and ignoring damping for now, combining (1.7) from (1.6) leads to,

$$\frac{1}{\gamma_1}\frac{d\boldsymbol{M}_1}{dt} + \frac{1}{\gamma_2}\frac{d\boldsymbol{M}_2}{dt} = -(\boldsymbol{M}_1 \times \boldsymbol{H}_{eff}) - (\boldsymbol{M}_2 \times \boldsymbol{H}_{eff}) \tag{1.8}$$

$$\frac{d\left(\frac{\boldsymbol{M}_1}{\gamma_1} + \frac{\boldsymbol{M}_2}{\gamma_2}\right)}{dt} = -\left((\boldsymbol{M}_1 + \boldsymbol{M}_2) \times \boldsymbol{H}_{eff}\right) \tag{1.9}$$

$$\frac{1}{\gamma_{eff}}\frac{d\boldsymbol{M}}{dt} = -(\boldsymbol{M} \times \boldsymbol{H}_{eff}) \tag{1.10}$$

Here $\boldsymbol{M} = \boldsymbol{M}_1 + \boldsymbol{M}_2$ is the net magnetization and the effective gyromagnetic ratio ${\gamma_{eff}}^2 = (\boldsymbol{M}_1 + \boldsymbol{M}_2)^2 / \left(\frac{\boldsymbol{M}_1}{\gamma_1} + \frac{\boldsymbol{M}_2}{\gamma_2}\right)^2$, giving $\gamma_{eff} = (M_1 - M_2)/\left(\frac{M_1}{\gamma_1} - \frac{M_2}{\gamma_2}\right)$. Now including damping, the net equation can be written:

$$\frac{d\boldsymbol{M}}{dt} = -\gamma_{eff}(\boldsymbol{M} \times \boldsymbol{H}_{eff}) + \frac{\alpha_1 M_1 \gamma_{eff}}{\gamma_1}\left(\hat{\boldsymbol{m}}_1 \times \frac{d\hat{\boldsymbol{m}}_1}{dt}\right) + \frac{\alpha_2 M_2 \gamma_{eff}}{\gamma_2}\left(\hat{\boldsymbol{m}}_2 \times \frac{d\hat{\boldsymbol{m}}_2}{dt}\right) \tag{1.11}$$

Due to antiferromagnetic coupling, $\hat{\boldsymbol{m}}_1 = -\hat{\boldsymbol{m}}_2 = \hat{\boldsymbol{m}}$. Therefore this equation becomes,

$$\frac{d\boldsymbol{M}}{dt} = -\gamma_{eff}(\boldsymbol{M} \times \boldsymbol{H}_{eff}) + \frac{\alpha_{eff}}{M_s}\left(\boldsymbol{M} \times \frac{d\boldsymbol{M}}{dt}\right) \tag{1.12}$$

Here M_s is the saturation magnetization which is equal to $(M_1 - M_2)$ and the effective damping constant $\alpha_{eff} = \left(\alpha_1 \frac{M_1}{\gamma_1} - \alpha_2 \frac{M_2}{\gamma_2}\right) / \left(\frac{M_1}{\gamma_1} - \frac{M_2}{\gamma_2}\right)$. The total angular momentum is written $J_i = \frac{M_i}{\gamma_i}$. The effective gyromagnetic ratio diverges as the net angular momentum goes to zero, increasing the precession rate. The effective damping constant, however, also diverges near the angular momentum compensation point. Examining the threshold current for anti-damping switching, one can notice that the threshold current would then also diverge, making switching a nearly compensated difficult unless the damping of the sublattices are small.

Antiferromagnetically-coupled materials have two resonance modes: ferromagnetic resonance (FMR) mode and exchange mode [43]. In the FMR mode, the coupled system is rigid and behaves as a ferromagnet with net magnetic moment equal to $(M_1 - M_2)$. In the exchange mode, the sublattices are canted away from the exchange field. In a perfect antiferromagnet, this canting produces a net magnetic moment. Typically, the FMR mode is responsible for switching times, which is proportional to $\gamma_{eff} H_k$ (H_k is the anisotropy field). Near the angular momentum compensation point it was shown that γ_{eff} increases (it decreases near the magnetization compensation). Looking at the anisotropy field, assuming an anisotropy energy k_u that does not change greatly near the compensation point, $H_k = 2k_u/M_s$. Therefore, near the compensation point the anisotropy field increases, and the FMR frequency is proportional to $(J_1 - J_2)^{-1}$, which diverges near the angular momentum compensation point, leading to faster dynamics.

Chapter 2

Spin-Orbit Torque Switching of Cobalt-Terbium Alloys

Recently, there has been a great interest in using antiferromagnetically coupled materials instead of ferromagnetic materials to store information. Compared with ferromagnetic materials, antiferromagnetically coupled systems exhibit much faster dynamics, which could potentially be used to increase the switching speeds of magnetic logic and memory devices, without necessarily increasing the switching current and energy [38,44]. Antiferromagnetically coupled systems also have the benefit of being robust against unwanted external magnetic fields, including fields from neighboring devices, which should be small if they are antiferromagnetic, and Oersted fields due to current. Overall, they promise to enable spintronic devices with higher speed and density.

Rare earth (RE)– *transition* metal (TM) ferrimagnetic alloys are one potential candidate material for realizing such devices. In RE-TM alloys, the magnetic moments of TM elements (such as Fe, Co, Ni) and the RE elements (e.g., Gd, Tb, Ho, etc.) can be aligned with anti-parallel orientations due to the exchange interaction between the 4f and 3d electrons in the rare earth and transition metal atoms [45]. By varying the relative concentrations of the two atomic species in the alloy, one can reach compensation points where the net magnetic moment or angular momentum goes to zero [46–49]. Moreover, because of the different origins of magnetism of the

two species, transport related properties, such as magnetoresistance and Hall effects, are dominated by TM moments in these alloys, providing a way to read out the magnetic state even in a compensated system. In contrast, in an antiferromagnet with symmetric sublattices, efficiently determining and distinguishing between bistable magnetic states can prove to be difficult.

In this chapter, we show that by utilizing current-induced spin-orbit torque of Ta, one can switch magnetic moments in $Ta/Co_{1-x}Tb_x$ bilayer films. Particularly, we found that effective fields generated from the spin-orbit torque scaled with the inverse of magnetization and reached maximum when the composition approaches the magnetic compensation point, which is consistent with angular momentum conservation. In addition, we also quantify the Dzyaloshinskii-Moriya interaction energy in the $Ta/Co_{1-x}Tb_x$ system and we find that the energy density increases as a function of the Tb concentration, which could be useful for generating stable magnetic textures. The large effective spin-orbit torque field magnetic field and the previously demonstrated fast dynamics near the magnetization and angular momentum compensation points [40,41] in these ferrimagnetic systems provide a promising platform for high speed and energy efficient spintronic applications. Part of the following sections is adapted from [50].

2.1 Magnetic Characterization and Device Fabrication

As discussed in the previous chapter, Spin-orbit torque (SOT) has proven to be an efficient method of controlling the ferromagnetic state of nanoscale devices [20,23,33,51]. SOT originates from spin-orbit interaction (SOI) induced spin generation in the bulk (i.e., the spin Hall effect) [15,16] or the surface (i.e., the Rashba-Edelstein effect) [17,18] of solid materials. Recently, it was demonstrated that one can use SOT to switch a TM-dominant CoFeTb ferrimagnet with bulk perpendicular magnetic anisotropy (PMA) [37]. It is therefore interesting to ask what the relationship is between the chemical composition of RE-TM alloys and the SOT efficiency, and whether or not one can switch a compensated (both magnetically and in angular momentum) ferrimagnet using SOT. To answer these questions, as shown in Fig. 2.1a, we grew a series of Ta(5)/$Co_{1-x}Tb_x$(t)/Ru(2) (thickness in nm) films using DC magnetron sputtering with base pressure ~1 x 10^{-8} Torr. Films were grown on Si substrates with 100 nm of wet thermally grown silicon oxide. In this film stack, Ta provides the SOT through the SHE and Ru is a capping layer to prevent oxidation of the magnetic layer. It is expected that the Ru layer will shunt some of the current. The $Co_{1-x}Tb_x$ alloys were deposited by co-sputtering Co and Tb sources with different sputtering powers. The power of Co was fixed, and the power of Tb was varied. The deposition time was kept constant for all samples, therefore the thickness of the samples increases slightly with increasing Tb deposition power. The concentration of Tb *x* was calculated from the

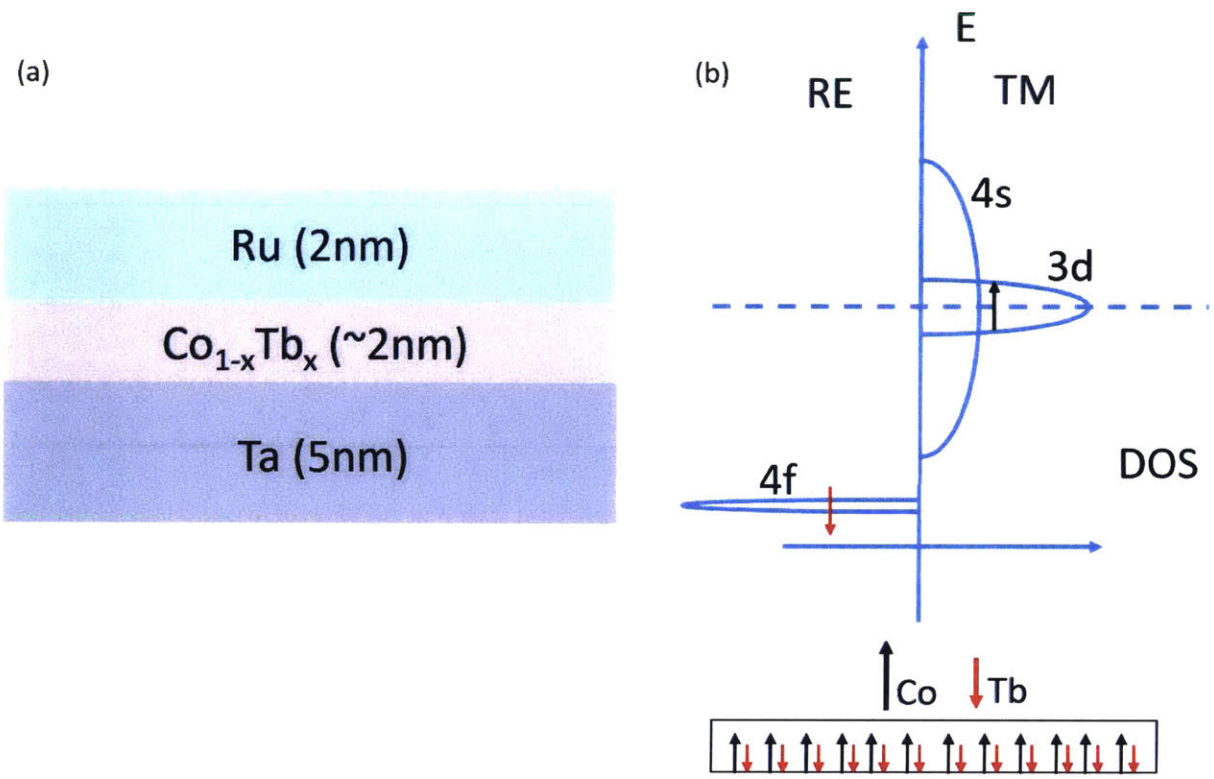

Figure 2.1: Film stack and cartoon density of states of CoTb. (a) Film stack deposited on silicon oxide. (b) Cartoon density of states demonstrating that the magnetism near the Fermi energy is dominated by the transition metal.

deposition rates and varied between 0.1 and 0.3, while the layer thickness *t* ranges from 1.7 nm to 2.6 nm.

The magnetic properties of the deposited films were examined using vibrating sample magnetometry (VSM), and PMA was observed for all samples [Fig. 2.2a]. In order to accurately determine the saturation magnetization, the area of the sample chip needed to be known. To figure this out, a standard silicon chip of known area was weighed. From the weight of the sample chips, the area is easily determined. Hard axis scans were also performed in order to determine the anisotropy field. Fig. 3 shows an example of a hard axis scan for a Co-dominant film with Tb

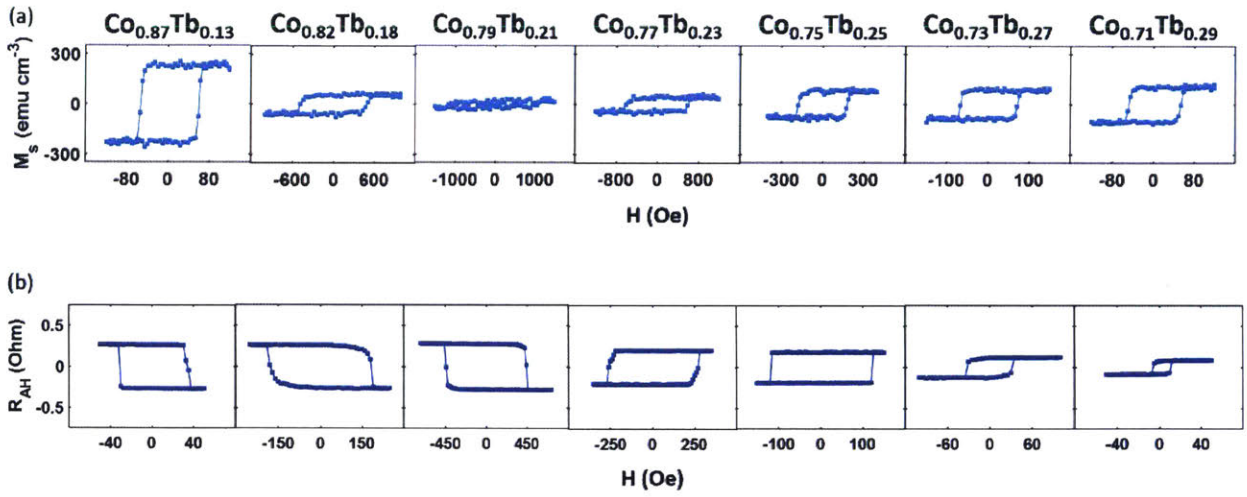

Figure 2.2: Magnetic Properties of $Co_{1-x}Tb_x$ Alloys. (a) Out of plane magnetization curves of $Co_{1-x}Tb_x$ films. (b) R_{AH} as a function of perpendicular magnetic field.

concentration $x = 0.13$. Only this film and the most Tb dominant film could be saturated along the hard axis due to the maximum field the VSM can apply (~1.4T). Furthermore, the magnetic moment goes through zero and the coercive fields reach their maximum around $x \approx 0.22$, which is consistent with the room temperature magnetic moment compensation point x_{cM} previously reported [48,49]. The dependence of the magnetic moment on the Tb concentration is summarized in Fig. 4a, which agrees well with the trend line calculated by assuming an anti-parallel alignment and locally linear relation between the Co and Tb moment (dashed lines).

Next, the samples were patterned into Hall bars with dimensions 4 x 44 μm^2 (Fig. 5). The fabrication process flow is summarized in Table 1. Generally, the process includes a two-step photolithography process. We found that ion-milling without a water cooled stage resulted in too much heating, causing the CoTb film to become non-magnetic. This is possibly due to Tb reacting with Ru or the oxygen in the RuO_x capping layer. Instead, a lift-off process was used to deposit the film stack. Once we obtained an ion-mill system with a water cooled stage, ion-milling

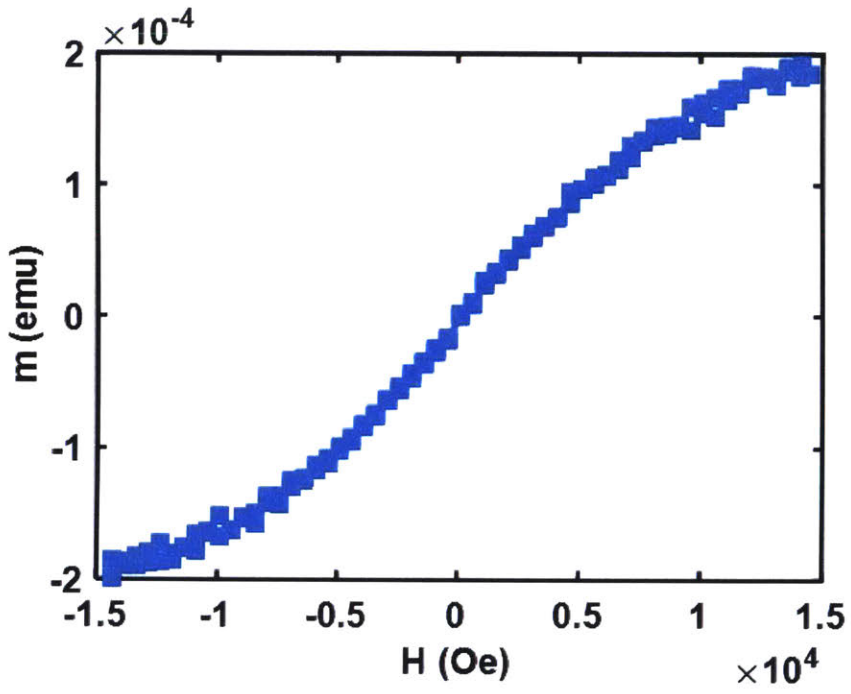

Figure 2.3: Hard axis measurement of $Co_{.87}Tb_{0.13}$.

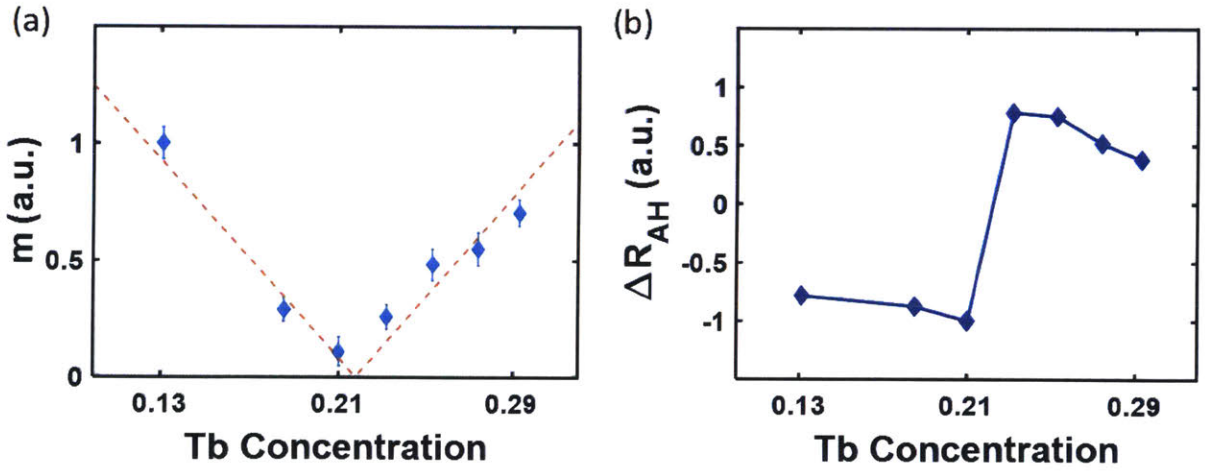

Figure 2.4: Summary of magnetic properties for $Co_{1-x}Tb_x$. (a) Magnetic moments of $Co_{1-x}Tb_x$ alloys as a function of Tb concentration. (b) R_{AH} as a function of Tb concentration.

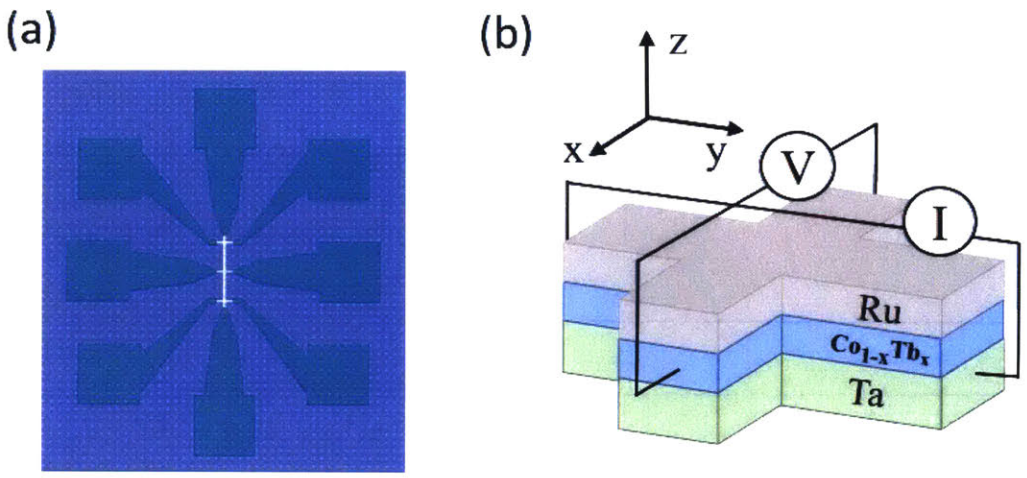

Figure 2.5: Hall bar device. (a) Layout of Hall bar contains multiple leads to measure resistance using 4-point measurement. (b) Geometry of device.

could be done without destroying the magnetism. The results in this chapter are based upon the lift-off process, but other work now uses an ion-mill process. Contacts were deposited using either evaporation of Ti/Au or sputtering of Ta/Ru. After fabrication the anomalous Hall resistance (R_{AH}) vs out of plane magnetic field H curves were measured for all samples (plotted in Fig. 2b and summarized in Fig. 4b. The cartoon band structure shown in Fig. 1b gives some insight into the magnetic properties of the CoTb alloy. The magnetism near the Fermi energy is dominated by the transition metal, while the magnetization of the rare earth atoms is localized to valence electrons, meaning the magneto-transport properties are dominated by the transition metal sublattice. The polarity of the hysteresis loops changes sign across x_{cM}, consistent with previous studies [52,53]. This sign change can be understood by following the Co moment in the alloy. For a Co-dominant film, the Co moments align with the external field to reduce the total energy. In a Tb-dominant film, the Tb moments align with the external field, causing the Co

moments to align in the opposite direction due to the antiferromagnetic exchange and the sign change in the R_{AH} hysteresis loops.

Step	Parameters
Spin AZ5214	3k rpm for 30s, bake 110C for 2 minutes
Expose MA4	3s
Hard Bake	2 minutes at 110C
Flood Exposure MA4	45s
Develop Az422	60s
Sputter film stack	
Lift-Off	Sonicate in Acetone or Microstrip 1 hour
Spin SPR 700	3k rpm for 30s, bake 110C for 2 minute
Expose MA4	6s
Develop CD-26	35s
Deposit Contacts and Lift-off	

Table 2.1: Fabrication flow.

2.2 Current-Induced Switching

After measuring field switching, next we measured the current-induced SOT switching. Fig. 2.6 illustrates the current-induced magnetic switching for the series of samples. During these measurements, in-plane magnetic fields of ±2000 Oe were applied in the applied electrical current direction [*y* axis in Fig. 2.5b]. Previous studies and the previous chapter have shown that an in-plane field is necessary to ensure deterministic magnetic switching of PMA films, because it can break the symmetry between two equivalent final states [22,25–27,54,55] . As shown in Fig. 2.6, the current-induced switching shows opposite polarities under the positive and negative applied fields, consistent with the model of SOT-induced switching of magnetic films with PMA [22]. Furthermore, under the same in-plane field, the switching polarity changes sign as the samples go from being Co-dominant to Tb-dominant. This phenomenon can be explained by considering a macrospin model as shown in Fig. 2.7. In SOT switching, the Slonczewski torque [5] is proportional to $\hat{\boldsymbol{m}} \times (\hat{\boldsymbol{\sigma}} \times \hat{\boldsymbol{m}})$, where $\hat{\boldsymbol{m}}$ is the unit vector along the magnetic moment direction and $\hat{\boldsymbol{\sigma}}$ is the orientation of electron spins generated from SOI [along the $\hat{\boldsymbol{x}}$ direction in Fig. 5b]. Because the torque is an even function of the local magnetic moment $\hat{\boldsymbol{m}}$, effects from both sublattices in the RE-TM alloy add constructively [38,56]. At equilibrium positions, $\hat{\boldsymbol{m}}$ and $\hat{\boldsymbol{\sigma}}$ are perpendicular to each other, and it is usually convenient to use an effective field [25] $H_{ST} \propto \hat{\boldsymbol{\sigma}} \times \hat{\boldsymbol{m}}$ to analyze the SOT effect on magnetic switching. The equilibrium position of $\hat{\boldsymbol{m}}$ can then be determined by balancing the anisotropy field H_{an}, the applied in-plane field H_y, and H_{ST}. As shown in Fig. 7,

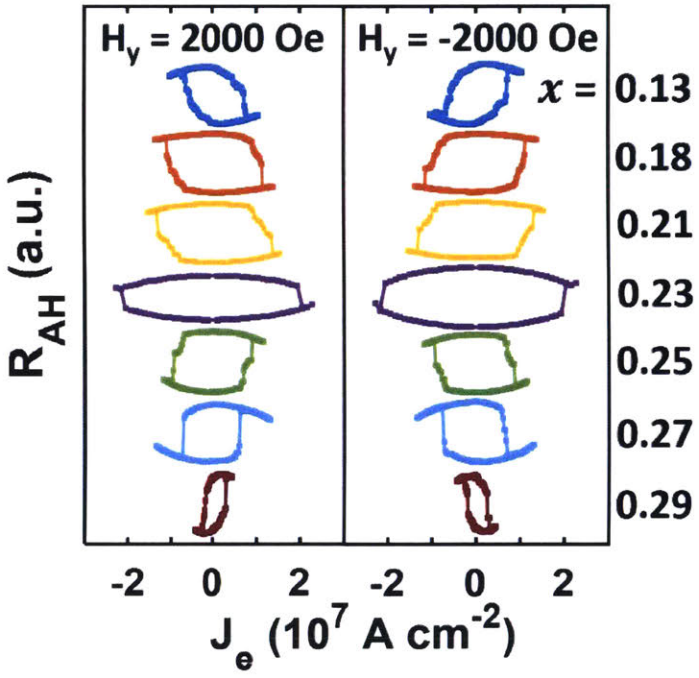

Figure 2.6: Current-induced switching. Current induced SOT switching of $Co_{1-x}Tb_x$ for in-plane fields of ± 2000 Oe. The current density inside Ta is calculated based on the conductivity of Ta thin films.

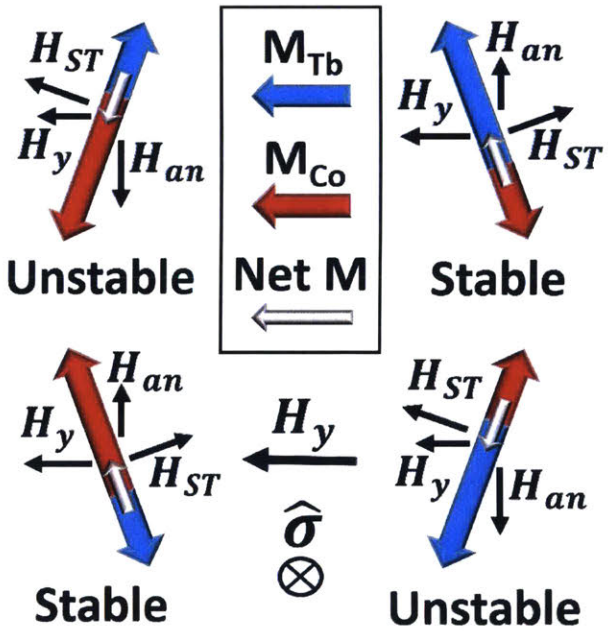

Figure 2.7: Ferrimagnetic switching phase diagram. Schematic of effective fields in a ferrimagnetic system. Fields acting on the moment consist of the in-plane field H_y, the anisotropy field H_{an}, and the SOT field H_{ST}.

when H_y and $\hat{\boldsymbol{\sigma}}$ are given by the illustrated directions, the final orientation of the Co sublattice magnetic moment will be close to the $+\hat{\boldsymbol{z}}$ direction for the Co dominant sample and close to the $-\hat{\boldsymbol{z}}$ direction for the Tb dominant sample, giving rise to opposite Hall voltages, similar to the case of field switching. Reversing H_y also reverses the direction the net moment will tilt towards, causing the equilibrium positions to flip, and the hysteresis loop to change signs. Based upon this analysis, the current induced switching should exhibit the same polarity change across the compensation point as the magnetic field induced switching. We note that all of the samples follow this rule except for the $Co_{0.77}Tb_{0.23}$ sample, where the field switching data had determined it to be Tb-dominant but the current induced switching corresponds to a Co-dominant sample. A careful study on this sample reveals that this change simply arises from Joule heating induced temperature change. In RE-TM alloys, the magnetic moments of the RE atoms have stronger temperature dependence compared with TM atoms. Consequently, when the temperature increases, a higher RE concentration is necessary to achieve the same magnetic moment compensation point [36,40,41,45–49]. This means that when samples that are slightly Tb-dominant are heated, they will cross the compensation point and become Co-dominant. By measuring the R_{AH} vs H curves of the $Co_{0.77}Tb_{0.23}$ sample under different applied currents, we found that the polarity of the field induced switching did change sign when the current density is higher than 2×10^7 A·cm^{-2}, suggesting at that current density, the sample reaches a temperature that passes the compensation temperature. The change from Tb-dominant to Co-dominant at this applied current density is a reversible change.

Overall the critical current values measured do not change greatly across the compensation point, even though the coercive fields do. This indicates it might be possible to

efficiently switch compensated films. To further explore, we use an experimental technique to directly measure the effective field induced by the spin torque.

2.3 Spin-Orbit-Torque Efficiency

The critical current of SOT induced switching in a multi-domain sample is influenced by defect-related factors such as domain nucleation and domain wall (DW) pinning [26]. Therefore, the SOT efficiency *cannot* be simply extracted using the critical current values determined in Fig. 2.6. To quantify the SOT in our samples more accurately, we measured the SOT induced effective field in the DW motion regime by comparing it with the applied perpendicular field, using the approach developed by C. F. Pai et al. [55]. It has been shown that in PMA films with Néel DWs, the Slonczewski term acts on the DW as an effective perpendicular magnetic field and induces DW motion [8] [25–27,54,55].Therefore, by measuring the current induced shift in the R_{AH} vs H_z curves, one can determine the magnitude of the SOT. Fig. 2.9 (a) and (b) show typical field induced switching curves for a Co-dominant sample $Co_{0.82}Tb_{0.18}$ and a Tb-dominant sample $Co_{0.75}Tb_{0.25}$. Under the applied current of ±3 mA and in-plane field of 2000 Oe, the centers of hysteresis loops are offset from zero, with opposite values for opposite

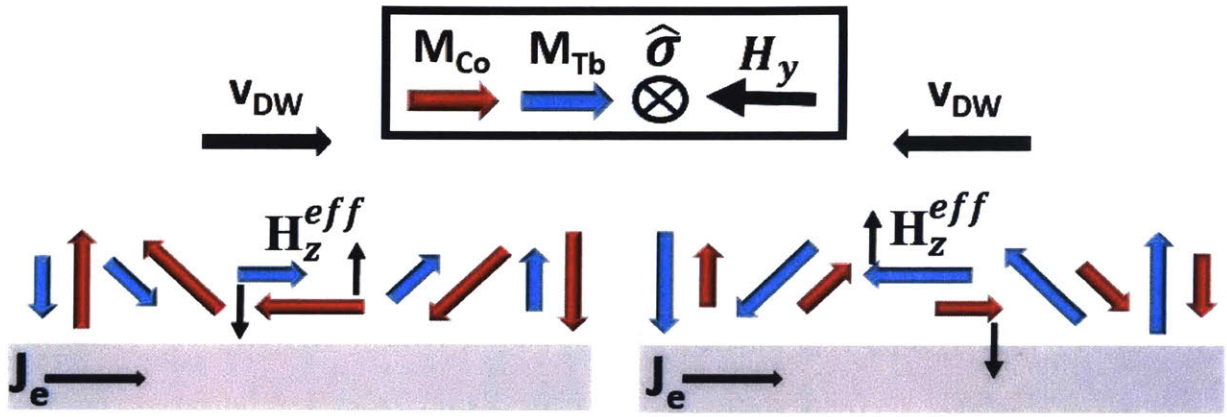

Figure 2.8: SOT induced DW motion in the ferrimagnetic system for Tb-dominant and Co-dominant films, showing that the effective perpendicular field has the same sign in both cases.

current directions. The current dependence of the offset fields are summarized in Fig. 2.9 (c) and (d) for $H_y = 0$ and ±2000 Oe, where a linear relationship between the offset field and the applied current is obtained. Note that this linear relationship only occurs at smaller current values where Joule heating does not play a role. This is because for simple Joule-heating induced coercive field changes has not effective on these measurements because the only thing we are concerned with is the center of the hysteresis loop, however for large Joule heating, the compensation point changes, which determines the strength of the SOT effective field.

In these plots, the ratio between the offset field H_z^{eff} and current density J_e curve represents the efficiency of the SOT at the Ta/RE-TM interface, defined as $\chi \equiv \frac{H_z^{eff}}{J_e}$. χ as a function of applied H_y for $Co_{0.82}Tb_{0.18}$ and $Co_{0.75}Tb_{0.25}$ samples are plotted in Fig. 2.9 (e) and (f), respectively. χ grows linearly in magnitude for small values of H_y, until reaching the saturation efficiency χ_{sat} at a large in-plane field H_y^{sat}. The evolution of χ as a function of H_y comes from the chirality change of the

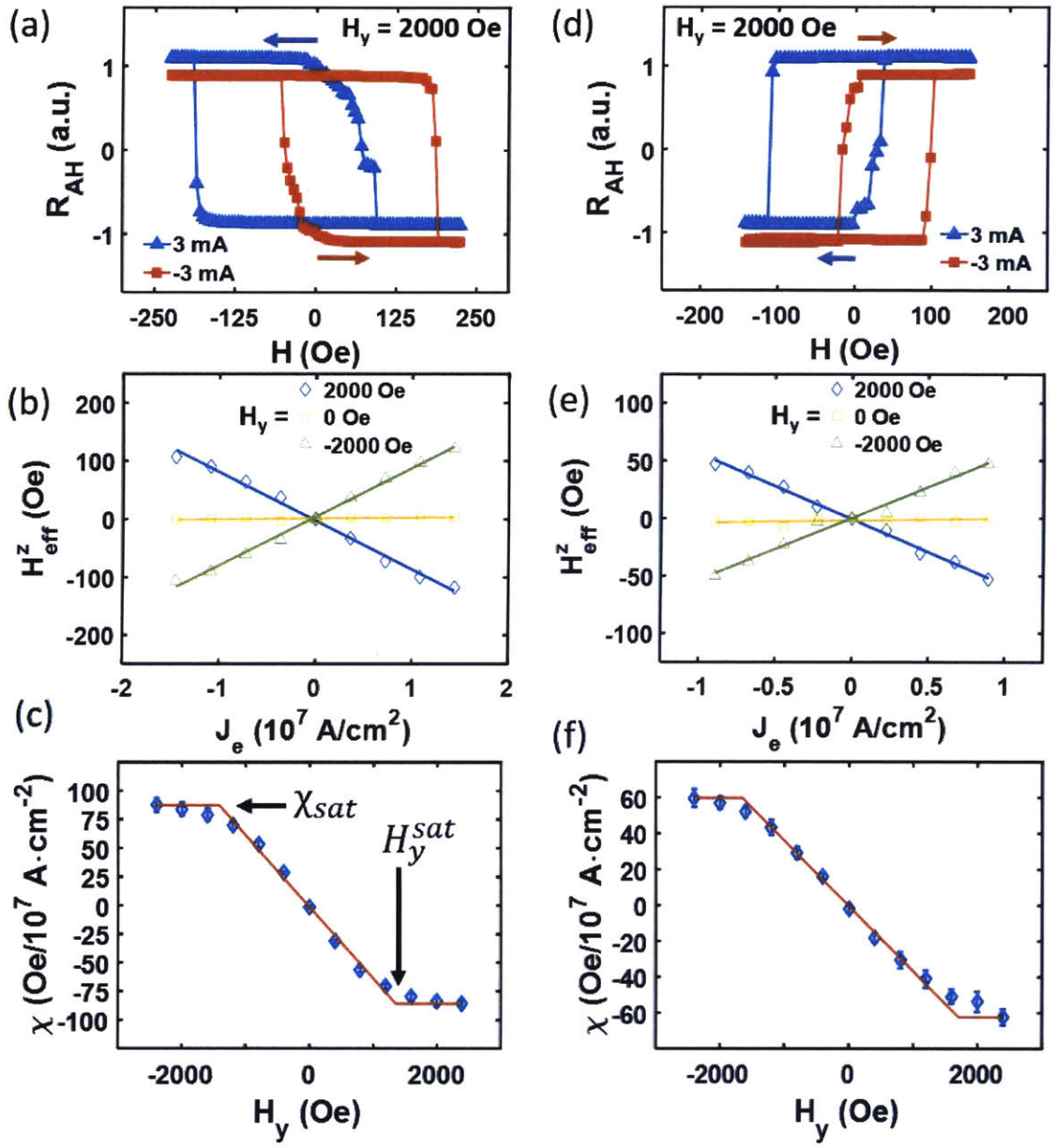

Figure 2.9 (a),(c),(e) Measurements on Co-dominant sample Co0.82Tb0.18. (b),(d),(f) Measurements on Tb-dominant sample Co0.75Tb0.25. (a),(b) RAH vs. applied perpendicular field under a DC current of ±3 mA. (c),(d) SOT effective field as a function of applied current density under in-plane fields of ±2000, and 0 Oe. (e),(f) SOT efficiency vs. Hy. Efficiency saturates at the field H_y^{sat}.

DWs in the sample. It is known that because of the *Dzyaloshinskii-Moriya interaction (DMI) mechanism* at the heavy metal/magnetic metal interface [28] or inside the bulk of RE-TM alloy [57], stable Néel DW with spontaneous chiralities are formed. Under zero H_y, the DWs do not favor either switching polarities, leading to a zero offset field. As H_y increases, the DMI induced effective field H_{DMI} is partially canceled, and DWs start to move in directions that enable magnetic switching. Therefore, H_y^{sat} represents the minimum field that is required to completely overcome H_{DMI} and χ_{sat} represents the maximum efficiency of the SOT for the given film concentration.

Fig. 2.10 illustrates the dependence of χ_{sat} on concentration x in the series of $Co_{1-x}Tb_x$ samples. It can be seen that χ_{sat} diverges near x_{CM}, with the largest value occurring for the sample with smallest magnetization. This result is consistent with the spin torque theory, where the ratio between the SOT effective field and applied charge current is $\chi_{sat} = (\pi/2)(\xi\hbar/2e\mu_0 M_s t)$ [55,58]. Here $\xi = {J_S}/{J_e}$ represents the effective spin Hall angle (combined effects of the spin Hall angle and spin-mixing conductance), $\frac{\hbar}{2e}J_s$ is the spin current density, $\hbar$ is Planck's constant, μ_0 is the vacuum permeability, and M_s is the saturation magnetization. Note that this model of spin torque is based upon the conservation of total angular momentum. Previously it has been suggested to utilize ferrimagnetic materials with minimized M_s to increase the efficiency of spin torque induced switching [59]. However, it was not verified if an efficient spin absorption could be achieved at the surface of a ferrimagnet material with antiparallel aligned

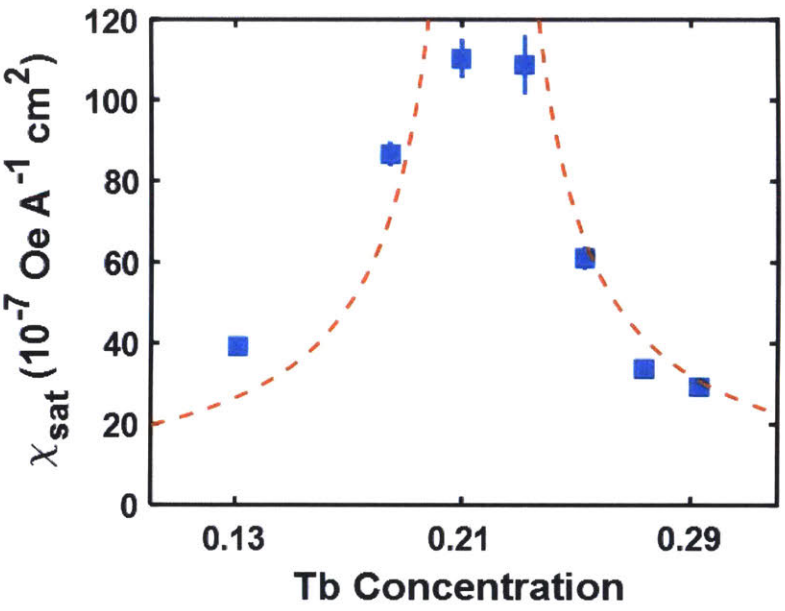

Figure SOT efficiency for different $Co_{1-x}Tb_x$ films : Saturation efficiency is largest near the magnetic moment compensation point. The dashed line in shows the trend calculated from χ_{sat} ~1/ $M_s t$.

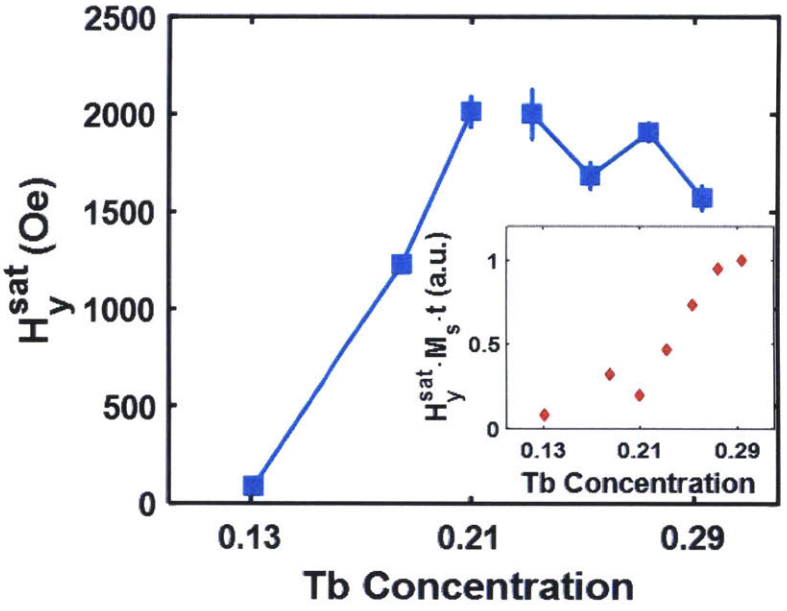

Figure 2.8 In-plane saturation field for different Co1-xTbx films.: The in-plane saturation field is largest near the magnetic moment compensation point. Inset plots the product of the in-plane saturation field and magnetic moment Mst, indicating an increase in DMI energy density D with increasing Tb concentration.

sublattices. Moreover, because of the mixture between the spin angular momentum and orbital angular momentum in RE-TM alloys, there have been debates over the conservation of total angular momentum in these systems [60]. Our experiment results provide clear evidence on the strong efficiency of spin orbit torques in antiferromagnetic coupled materials. Within the experimental accuracy, we found that the effective field from the SOT does follow the simple trend given by $1/M_S t$ [dashed lines in Fig. 2.10], reflecting total angular momentum conservation. ξ in our samples is determined to be ~0.03, smaller than previously reported values from Ta/magnetic layer devices, possibly due to the relatively smaller spin-mixing conductance at the Ta/CoTb interface [61].

In addition to the magnetic moment compensation point x_{cM}, RE-TM systems also possess an angular momentum compensation point x_{cJ} due to the different g factors associated with spin and orbit angular moment. For our $Co_{1-x}Tb_x$ system, using the g factors of Co (~2.2) and Tb (~1.5) atoms [62,63] , along with the relation $J_{Co(Tb)} = M_{Co(Tb)}/\gamma_{Co(Tb)}$, where $\gamma_{Co(Tb)} = -g_{Co(Tb)}\mu_B/\hbar$ (μ_B being the Bohr magneton, $\gamma_{Co(Tb)}$ the gyromagnetic ratio, and $J_{Co(Tb)}$ the total angular momentum per unit volume), we determine x_{cJ} to be ~17% (based upon the magnetic compensation point), which is within the range of the studied samples and lower than x_{cM}. Previously it was demonstrated that ultrafast field-driven magnetic dynamics could be excited around x_{cJ} [40,41]. According to Landau-Lifshitz-Gilbert equation of a ferrimagnetic system [5,36,42], the spin torque term leads to $\frac{d\hat{\boldsymbol{m}}}{dt} \sim -\gamma_{eff}\frac{\hbar J_S}{2e\mu_0 M_S t}(\hat{\boldsymbol{m}} \times \hat{\boldsymbol{\sigma}} \times \hat{\boldsymbol{m}})$, where $\gamma_{eff} = (M_{Co} - M_{Tb})/(J_{Co} - J_{Tb})$ (derived in previous chapter) is the effective gyromagnetic ratio and $M_S = M_{Co} - M_{Tb}$ [40,41]. When $J_{Co} - J_{Tb}$ approaches zero, the time evolution of $\hat{\boldsymbol{m}}$ diverges if J_s remains finite at x_{cJ}. As observed in Fig. 2.10, χ_{sat} remains roughly unchanged

across x_{cJ}, suggesting that similar to the field-driven experiment, SOT could also be used as an efficient drive force for achieving fast dynamics at this concentration.

We also find that the switching polarity keeps the same sign across x_{cJ}, differing from the current induced switching of CoGd spin valves studied in Ref. [29], where a switching polarity reversal was observed between x_{cJ} and x_{cM}. This difference is due to the presence of different switching mechanisms: in SOT induced switching of PMA films, the two competing torques are the field torque $\gamma_{eff}\boldsymbol{M} \times \boldsymbol{H}_{eff}$ and the spin torque. Because the two terms have the same pre-factor γ_{eff} and are only functions of $\boldsymbol{M}$, $\boldsymbol{H}_{eff}$, and $\hat{\boldsymbol{\sigma}}$, under the same applied $\hat{\boldsymbol{\sigma}}$ and $\boldsymbol{H}_y$, the orientation of $\hat{\boldsymbol{m}}$ will remain the same (Fig. 2.7), regardless of the sign of γ_{eff}. In contrast, the anti-damping switching of spin valves changes polarity for regions with $\gamma_{eff} < 0$, as explained in Ref. [29].

The in-plane field needed for saturating the SOT and overcoming the DMI field, H_y^{sat}, is plotted against the Tb concentration in Fig. 2.11. First, we notice that H_y^{sat} is largest near x_{cM}. This result is consistent with fact that the effective DMI field [58] $H_{DMI} = D/M_s t\mu_0\Delta$, where D is the DMI energy density and Δ is the DW width, would become divergent when M_s approaches zero. Secondly, H_y^{sat} is generally larger for the Tb-dominant samples than the Co-dominant ones. For example, the sample with the highest Co concentration, $Co_{0.87}Tb_{0.13}$, shows H_y^{sat}~100 Oe, which is close to the reported saturation field of Ta/FM stacks [55]. However, in the Tb dominant sample $Co_{0.71}Tb_{0.29}$, which has similar magnetic moment, H_y^{sat} is found to be ~1500 Oe. In the inset of Fig. 2.11 we plot $H_y^{sat}M_s t$, which increases roughly linearly as a function of x. By calculating the DW width $\Delta = \sqrt{A/K_u}$ using the determined anisotropy energy K_u = 6.4 × 10^4

$J \cdot m^{-2}$ from Tb- and Co-dominant samples anisotropy fields and the reported exchange stiffness [64] $A \sim 1.4 \times 10^{-11}$ J/m, we find *D* to be in the range of 0.05~0.66 pJ/m. The increasing DMI energy with increasing Tb concentration can be explained by the strong spin-orbit coupling and large deviation from the free electron g factor [28] in the Tb atoms. The generation of magnetic textures such as chiral DWs and magnetic skyrmions [65] relies on the competition between the DMI energy and other magnetostatic energies. Therefore, the tunable DMI through chemical composition provides a useful a knob for controlling magnetic phases.

Chapter 3

Conclusion

Although the future of computing technology is uncertain, spintronic-based devices promise energy efficient alternatives going forward. However, realizing such devices requires further work on reducing the switching time and critical currents in these devices, for both logic and memory applications. In this work, a general overview of spin torque, including spin-transfer torque and spin-orbit torque was presented. The critical current and switching times were explored, and it was shown that antiferromagnetically coupled materials are promising candidates for improving the performance of spintronic devices. This was further demonstrated with a general analysis of antiferromagnetically coupled systems dynamics and discussion on what some of the benefits and difficulties would be in using such a system.

In the next chapter, an antiferromagnetically coupled system was experimentally invested. We were able to demonstrate SOT-induced switching of $Co_{1-x}Tb_x$ thin films with PMA over a wide range of chemical compositions. The effective field from the SOT was found to scale with the inverse of magnetic moment, consistent with the conservation of angular momentum. The high efficiency of SOT at the compensation points as well as the previously demonstrated fast dynamics in these systems makes them highly attractive for high speed spintronic applications. Moreover, we found that the DMI energy density is much larger in samples with high rare earth concentrations, which could provide useful applications in spintronic devices

that employ stable magnetic textures. Beyond examining the steady state switching, future studies are needed to explore the potentially fast dynamics near the compensation points.

References

[1] D. E. Nikonov and I. A. Young, in *2012 Int. Electron Devices Meet.* (2012), p. 25.4.1-25.4.4.

[2] A. D. Kent and D. C. Worledge, Nat. Nanotechnol. **10**, 187 (2015).

[3] K.-H. Kim, S. Gaba, D. Wheeler, J. M. Cruz-Albrecht, T. Hussain, N. Srinivasa, and W. Lu, Nano Lett. **12**, 389 (2012).

[4] S. H. Jo, T. Chang, I. Ebong, B. B. Bhadviya, P. Mazumder, and W. Lu, Nano Lett. **10**, 1297 (2010).

[5] J. C. Slonczewski, "Current-driven excitation of magnetic multilayers," J. Magn. Magn. Mater. 159, L1 (1996).

[6] L. Berger, Phys. Rev. B **54**, 9353 (1996).

[7] E. B. Myers, D. C. Ralph, J. A. Katine, R. N. Louie, and R. A. Buhrman, Science **285**, 867 (1999).

[8] J. A. Katine, F. J. Albert, R. A. Buhrman, E. B. Myers, and D. C. Ralph, Phys. Rev. Lett. **84**, 3149 (2000).

[9] Appl. Phys. Lett. **84**, 3118 (2004).

[10] G. S. D. Beach, M. Tsoi, and J. L. Erskine, J. Magn. Magn. Mater. **320**, 1272 (2008).

[11] D. C. Ralph and M. D. Stiles, J. Magn. Magn. Mater. **320**, 1190 (2008).

[12] J. Z. Sun, Phys. Rev. B **62**, 570 (2000).

[13] O. J. Lee, V. S. Pribiag, P. M. Braganca, P. G. Gowtham, D. C. Ralph, and R. A. Buhrman, Appl. Phys. Lett. **95**, 012506 (2009).

[14] A. D. Kent, B. Özyilmaz, and E. del Barco, Appl. Phys. Lett. **84**, 3897 (2004).

[15] M. I. Dyakonov and V. I. Perel, "Current-induced spin orientation of electrons in semiconductors," Phys. Lett. A 35, 459 (1971).

[16] J. E. Hirsch, "Spin Hall Effect," Phys. Rev. Lett. 83, 1834 (1999).

[17] Y. A. Bychkov and E. I. Rashba,"Properties of a 2D electron gas with lifted spectral degeneracy," JETP Lett 39, 78 (1984).

[18] V. M. Edelstein,"Spin polarization of conduction electrons induced by electric current in two-dimensional asymmetric electron systems," Solid State Commun. 73, 233 (1990).

[19] J. Sinova, S. O. Valenzuela, J. Wunderlich, C. H. Back, and T. Jungwirth, Rev. Mod. Phys. **87**, 1213 (2015).

[20] L. Liu, C.-F. Pai, Y. Li, H. W. Tseng, D. C. Ralph, and R. A. Buhrman,"Spin-Torque Switching with the Giant Spin Hall Effect of Tantalum," Science 336, 555 (2012).

[21] C.-F. Pai, L. Liu, Y. Li, H. W. Tseng, D. C. Ralph, and R. A. Buhrman, Appl. Phys. Lett. **101**, 122404 (2012).

[22] L. Liu, O. J. Lee, T. J. Gudmundsen, D. C. Ralph, and R. A. Buhrman, "Current-Induced Switching of Perpendicularly Magnetized Magnetic Layers Using Spin Torque from the Spin Hall Effect," Phys. Rev. Lett. 109, 96602 (2012).

[23] I. M. Miron, K. Garello, G. Gaudin, P.-J. Zermatten, M. V. Costache, S. Auffret, S. Bandiera, B. Rodmacq, A. Schuhl, and P. Gambardella, "Perpendicular switching of a single ferromagnetic layer induced by in-plane current injection," Nature 476, 189 (2011).

[24] I. Mihai Miron, G. Gaudin, S. Auffret, B. Rodmacq, A. Schuhl, S. Pizzini, J. Vogel, and P. Gambardella, Nat. Mater. **9**, 230 (2010).

[25] S. Emori, U. Bauer, S.-M. Ahn, E. Martinez, and G. S. D. Beach,"Current-driven dynamics of chiral ferromagnetic domain walls," Nat. Mater. 12, 611 (2013).

[26] O. J. Lee, L. Q. Liu, C. F. Pai, Y. Li, H. W. Tseng, P. G. Gowtham, J. P. Park, D. C. Ralph, and R. A. Buhrman,"Central role of domain wall depinning for perpendicular magnetization switching driven by spin torque from the spin Hall effect," Phys. Rev. B 89, 24418 (2014).
[27] P. P. J. Haazen, E. Murè, J. H. Franken, R. Lavrijsen, H. J. M. Swagten, and B. Koopmans, "Domain wall depinning governed by the spin Hall effect," Nat. Mater. 12, 299 (2013).
[28] T. Moriya, "Anisotropic Superexchange Interaction and Weak Ferromagnetism," Phys. Rev. 120, 91 (1960).
[29] G. Yu, P. Upadhyaya, Y. Fan, J. G. Alzate, W. Jiang, K. L. Wong, S. Takei, S. A. Bender, L.-T. Chang, Y. Jiang, M. Lang, J. Tang, Y. Wang, Y. Tserkovnyak, P. K. Amiri, and K. L. Wang, Nat. Nanotechnol. **9**, 548 (2014).
[30] Y.-C. Lau, D. Betto, K. Rode, J. M. D. Coey, and P. Stamenov, Nat. Nanotechnol. **11**, 758 (2016).
[31] S. Fukami, C. Zhang, S. DuttaGupta, A. Kurenkov, and H. Ohno, Nat. Mater. **15**, 535 (2016).
[32] A. R. Mellnik, J. S. Lee, A. Richardella, J. L. Grab, P. J. Mintun, M. H. Fischer, A. Vaezi, A. Manchon, E.-A. Kim, N. Samarth, and D. C. Ralph, Nature **511**, 449 (2014).
[33] Y. Fan, P. Upadhyaya, X. Kou, M. Lang, S. Takei, Z. Wang, J. Tang, L. He, L.-T. Chang, M. Montazeri, G. Yu, W. Jiang, T. Nie, R. N. Schwartz, Y. Tserkovnyak, and K. L. Wang,"Magnetization switching through giant spin–orbit torque in a magnetically doped topological insulator heterostructure," Nat. Mater. 13, 699 (2014).
[34] L. Liu, A. Richardella, I. Garate, Y. Zhu, N. Samarth, and C.-T. Chen, Phys. Rev. B **91**, 235437 (2015).
[35] K. Garello, C. O. Avci, I. M. Miron, M. Baumgartner, A. Ghosh, S. Auffret, O. Boulle, G. Gaudin, and P. Gambardella, Appl. Phys. Lett. **105**, 212402 (2014).
[36] X. Jiang, L. Gao, J. Z. Sun, and S. S. P. Parkin, "Temperature Dependence of Current-Induced Magnetization Switching in Spin Valves with a Ferrimagnetic CoGd Free Layer," Phys. Rev. Lett. 97, 217202 (2006).
[37] Z. Zhao, M. Jamali, A. K. Smith, and J.-P. Wang,"Spin Hall switching of the magnetization in Ta/TbFeCo structures with bulk perpendicular anisotropy," Appl. Phys. Lett. 106, 132404 (2015).
[38] T. Jungwirth, X. Marti, P. Wadley, and J. Wunderlich, "Antiferromagnetic spintronics," Nat. Nanotechnol. 11, 231 (2016).
[39] A. V. Kimel, A. Kirilyuk, A. Tsvetkov, R. V. Pisarev, and T. Rasing, Nature **429**, 850 (2004).
[40] C. D. Stanciu, A. V. Kimel, F. Hansteen, A. Tsukamoto, A. Itoh, A. Kirilyuk, and T. Rasing,"Ultrafast spin dynamics across compensation points in ferrimagnetic GdFeCo: The role of angular momentum compensation," Phys. Rev. B 73, 220402 (2006).
[41] M. Binder, A. Weber, O. Mosendz, G. Woltersdorf, M. Izquierdo, I. Neudecker, J. R. Dahn, T. D. Hatchard, J.-U. Thiele, C. H. Back, and M. R. Scheinfein, "Magnetization dynamics of the ferrimagnet CoGd near the compensation of magnetization and angular momentum," Phys. Rev. B 74, 134404 (2006).
[42] R. K. Wangsness,"Sublattice Effects in Magnetic Resonance," Phys. Rev. 91, 1085 (1953).
[43] F. Keffer and C. Kittel, Phys. Rev. **85**, 329 (1952).
[44] C. Marrows, "Addressing an antiferromagnetic memory," Science 351, 558 (2016).
[45] I. A. Campbell,"Indirect exchange for rare earths in metals", J. Phys. F Met. Phys. 2, L47 (1972).

[46] K. Lee and N. Heiman,"Magnetism in rare earth-transition metal amorphous alloy films," in AIP Conf. Proc. (AIP Publishing, 1975), pp. 108–109.
[47] K. H. J. Buschow,"Magnetic properties of amorphous rare-earth–cobalt alloys," J. Appl. Phys. 51, 2795 (1980).
[48] Y. J. Choe, S. Tsunashima, T. Katayama, and S. Uchiyama, "Magneto-optic Kerr spectra of amorphous RE-Co thin films," J. Magn. Soc. Jpn. 11, S1_273 (1987).
[49] P. Hansen, C. Clausen, G. Much, M. Rosenkranz, and K. Witter, "Magnetic and magneto-optical properties of rare-earth transition-metal alloys containing Gd, Tb, Fe, Co," J. Appl. Phys. 66, 756 (1989).
[50] J. Finley and L. Liu, Phys. Rev. Appl. **6**, 054001 (2016).
[51] H. Kurebayashi, J. Sinova, D. Fang, A. C. Irvine, T. D. Skinner, J. Wunderlich, V. Novák, R. P. Campion, B. L. Gallagher, E. K. Vehstedt, L. P. Zârbo, K. Výborný, A. J. Ferguson, and T. Jungwirth,"An antidamping spin-orbit torque originating from the Berry curvature," Nat. Nanotechnol. 9, 211 (2014).
[52] Y. Mimura, N. Imamura, and Y. Kushiro,"Hall effect in rare-earth–transition-metal amorphous alloy films," J. Appl. Phys. 47, 3371 (1976).
[53] N. Nagaosa, J. Sinova, S. Onoda, A. H. MacDonald, and N. P. Ong,"Anomalous Hall effect," Rev. Mod. Phys. 82, 1539 (2010).
[54] S. Emori, E. Martinez, K.-J. Lee, H.-W. Lee, U. Bauer, S.-M. Ahn, P. Agrawal, D. C. Bono, and G. S. D. Beach,"Spin Hall torque magnetometry of Dzyaloshinskii domain walls," Phys. Rev. B 90, 184427 (2014).
[55] C.-F. Pai, M. Mann, A. J. Tan, and G. S. D. Beach, "Determination of spin torque efficiencies in heterostructures with perpendicular magnetic anisotropy," Phys. Rev. B 93, 144409 (2016).
[56] H. V. Gomonay and V. M. Loktev, "Spin transfer and current-induced switching in antiferromagnets," Phys. Rev. B 81, 144427 (2010).
[57] T. Tono, T. Taniguchi, K.-J. Kim, T. Moriyama, A. Tsukamoto, and T. Ono, "Chiral magnetic domain wall in ferrimagnetic GdFeCo wires," Appl. Phys. Express 8, 73001 (2015).
[58] A. Thiaville, S. Rohart, É. Jué, V. Cros, and A. Fert, "Dynamics of Dzyaloshinskii domain walls in ultrathin magnetic films," EPL Europhys. Lett. 100, 57002 (2012).
[59] J. Z. Sun and D. C. Ralph,"Magnetoresistance and spin-transfer torque in magnetic tunnel junctions," J. Magn. Magn. Mater. 320, 1227 (2008).
[60] P. M. Haney, R. A. Duine, A. S. Núñez, and A. H. MacDonald,"Current-induced torques in magnetic metals: Beyond spin-transfer," J. Magn. Magn. Mater. 320, 1300 (2008).
[61] C.-F. Pai, Y. Ou, L. H. Vilela-Leão, D. C. Ralph, and R. A. Buhrman,"Dependence of the efficiency of spin Hall torque on the transparency of Pt/ferromagnetic layer interfaces," Phys. Rev. B 92, 64426 (2015).
[62] B. I. Min and Y.-R. Jang, "The effect of the spin-orbit interaction on the electronic structure of magnetic materials," J. Phys. Condens. Matter 3, 5131 (1991).
[63] J. M. D. Coey, *Rare-Earth Iron Permanent Magnets* (Clarendon Press, 1996).
[64] J. J. Turner, X. Huang, O. Krupin, K. A. Seu, D. Parks, S. Kevan, E. Lima, K. Kisslinger, I. McNulty, R. Gambino, S. Mangin, S. Roy, and P. Fischer, "X-Ray Diffraction Microscopy of Magnetic Structures," Phys. Rev. Lett. 107, 33904 (2011).

[65] X. Z. Yu, Y. Onose, N. Kanazawa, J. H. Park, J. H. Han, Y. Matsui, N. Nagaosa, and Y. Tokura,"Real-space observation of a two-dimensional skyrmion crystal," Nature 465, 901 (2010).